

Conducting atomic force microscopy for nanoscale tunnel barrier characterization

K. M. Lang, D. A. Hite, R. W. Simmonds, R. McDermott, D. P. Pappas,
and John M. Martinis
National Institute of Standards and Technology, 325 Broadway,
Boulder, CO 80305, USA

Increasing demands on nanometer-scale properties of oxide tunnel barriers necessitate a consistent means to assess them at these lengths. Here we use conducting atomic force microscopy (CAFM) to characterize aluminum oxide (AlO_x) barriers to be used in Josephson-junction qubits. We find the appropriate physical interpretation for CAFM is as a probe of local propensity for insulator breakdown. We consider the effect of imaging force to establish a statistically reproducible method to compare CAFM current maps. We present results for several AlO_x samples demonstrating the potential of this technique.

I. Introduction

Planar tunnel junctions are ubiquitous in solid state devices. Superconducting Josephson-junctions as quantum bits (JJ-qubits), magnetic tunnel junctions for magnetic random access memory (MRAM), and metal-oxide-semiconductor (MOS) devices constitute contemporary applications of oxide-barrier planar tunnel junctions. As the performance standards for these devices become more stringent, the properties of the oxide barrier become more vital. For MOS devices, as sizes become smaller and the gate oxides correspondingly thinner, atomic-scale defects may play a role in determining insulator breakdown [1]. In JJ-qubits it has recently been suggested that fluctuations in the local conductance of the oxide barrier can couple to the quantum bit, leading to decoherence [2].

Scanned-probe techniques provide a means to study oxide barriers at the nanometer scale. Scanning tunneling microscopy (STM) [3,4], ballistic electron emission microscopy (BEEM) [5], scanning capacitance microscopy (SCM) [6], and conducting atomic force microscopy (CAFM) [7,8,9,10,11] have all been used to study the local properties of oxide barriers used in planar junctions. Of these and other available scanned probe techniques, CAFM offers significant advantages for the study of insulating materials at the nanometer scale because it combines relatively-high (~ 20 nm) spatial resolution with the ability to both scan and take conductivity maps at any applied bias voltage, including those inside the insulating gap.

Despite these advantages and the fact that CAFM has been available for a decade, this technique has not been widely used. We suggest this is due to the difficulty of achieving reproducible measurements with CAFM, given the large number of factors that may influence the images. These include tip material and wear properties, ambient environment, and the imaging force. In addition, the issues of appropriate interpretation and use of CAFM images need to be addressed. While some work has been done to address these problems [12,13,14], a consensus is required on appropriate imaging conditions and interpretation to render CAFM a more standard and powerful characterization tool.

In this paper we report conducting atomic force microscopy results on a common tunnel-barrier material, aluminum oxide (AlOx), with a particular emphasis on developing reproducible imaging conditions and appropriate interpretation. We find that control of the imaging force is a critical factor for reproducibility, and we suggest that the significant disparities between previously published CAFM measurements on comparable AlOx samples [7,8,9,10] can be explained by differences in this variable. We further find that CAFM measurements under the usual imaging conditions do not generally probe intrinsic local conductance, as implied in previous papers, but rather actually probe the local propensity for insulator breakdown, which we term the *pinhole susceptibility*. This is a new interpretation of the physics involved in conducting atomic force microscopy on these materials.

Although the discussion and data presented herein focus on one particular material, the applicability of these results is more generic. We began this study because we currently use AlOx as the tunnel barrier in our Josephson-junction quantum bits [15], and we now believe that materials properties are a significant limiting factor in achieving longer coherence times [2]. We are working to use CAFM to qualitatively and rapidly evaluate and rank the relative merits of new fabrication methods and materials without having to produce and test final devices. Independent of the material under study, consistent evaluation (or intercomparison between independent experiments) requires reproducibility, which in turn requires recognition of imaging force as a critical variable. We are also using CAFM to understand the connection between the nanoscale tunnel-barrier characteristics and macroscopic device performance. Again, independent of the material under study, understanding this connection requires an appropriate interpretation of the physical mechanism involved in the technique. We reiterate that CAFM is a highly appropriate technique for characterizing insulating tunnel-barrier materials, provided that generic issues of reproducibility and interpretation such as those discussed in this paper can be addressed.

II. Experimental Method

For all measurements we use a Digital Instruments/Veeco Metrology Nanoscope IIIa-Dimension 3000 atomic force microscope with standard CAFM upgrade [16]. The two significant parameters for these measurements are the lateral spatial resolution and the minimum measurable current. The lateral spatial resolution of the instrument is highly

tip-dependent, and for the tips used in this study is approximately 20 nm. The minimum detectable signal from the current amplifier is about 1 pA.

A wide variety of cantilevers are available for this instrument. For these measurements, we use silicon cantilevers with a 60-140 nm coating of platinum/iridium and a final end radius of 20-40 nm (DI/Veeco SCM-PIT) [16]. The spring constant of these cantilevers is nominally 2.8 N/m; however, this value can vary from 1 N/m - 5 N/m for cantilevers fabricated on different wafers and by $\pm 10\%$ for cantilevers from a single wafer. Tips were judged to be acceptable if they: (1) produced stable topographies showing features comparable in size to the tip radius; (2) measured current features of appropriate magnitude on a control sample (Table I: s2); (3) showed deflection/displacement curves comparable to that of the Fig. 2a inset. We found that tips could satisfy these requirements for 15 – 20 scan hours.

All samples studied in this paper consist of the following layers: Si + (optional) SiO₂ + 100 nm Al + AlOx. Table I gives details of sample fabrication. The Al was deposited at room temperature in a vacuum chamber (base pressure 1.3×10^{-5} Pa [1×10^{-7} torr]). The AlOx barrier was then formed on the bare Al by using a controlled exposure (2 min at 0.1 Pa [0.8 millitorr] followed by 10 min at 1.3 kPa [10 torr]) of pure oxygen at room temperature. After oxidation, the samples were removed from the vacuum chamber and imaged in air at room temperature. An initial image was generally taken within 10 minutes of the sample being exposed to air. Samples were then stored in air, and were imaged periodically over weeks and months subsequent to their fabrication.

In order to achieve consistency in our measurements, the protocol for all data presented in this paper is as follows. The rationale for this protocol will be subsequently clarified. Measurements were made in contact mode at constant force. The imaging force was checked before and after every image by acquisition of a deflection/displacement curve such as that seen in the inset to Fig. 2a. The imaging force is then given by $F = k x$, where k is the spring constant of the current cantilever and x is the deflection feedback setpoint. All data presented in this paper were taken at a time which was many oxidation time constants after the samples were fabricated, and on an area that had never been scanned before (unless otherwise stated).

III. Results and Discussion

In Fig. 1 we present topographies and current maps for the three samples described in Table I. The topographic roughness for each sample is given in Table I. Figs. 1d and 1h give histograms of the current maps. All the data in these figures were taken with the same cantilever and on the same day. Focusing on the current maps, much of the scanned area shows a current less than the 1 pA sensitivity of the amplifier (green areas). The regions of the current maps showing a local maximum of the measured current (red areas) are hereby functionally defined as *pinholes*. It is the characterization of these regions which is the focus of this paper.

In the simplest model, the CAFM tip can be considered as a small junction counter-electrode, and thus its spatially averaged resistance-area product should be comparable to that of a larger device with the same insulating barrier. For $100 \mu\text{m}^2$ area Al-AlO_x-Al junctions with comparable barriers to those of Fig. 1, we measure a resistance of $10 - 100 \Omega$ which gives a resistance-area (RA) product of $10^3 - 10^4 \Omega \mu\text{m}^2$. However, as seen in the figure, with the CAFM tip on average we measure currents of order tens of pA with a bias of -1 V. Given our nominal tip radius of tens of nm, this gives an RA product of order $10^7 - 10^8 \Omega \mu\text{m}^2$. To achieve RA products comparable to the larger junctions, we would need to assume a tip-sample contact radius of order 0.1 nm. As this seems physically unreasonable, we need to further assess the significance of the measured pinholes.

To elucidate the origin of the observed pinholes and to assess the effect of imaging in air, we performed the following experiment. Looking at samples fabricated weeks before study and stored in air, we tracked individual pinholes in sequential images of the same area and observed the pinholes disappeared in time. The elapsed time before they were no longer visible given the 1 pA noise floor of our current amplifier was $\sim 10-30$ minutes for all three samples of Table I. When the percentage of oxygen was lowered from 20 % (air) to 5 % by continuous flow of N₂ in the semi-sealed AFM chamber, we found that the disappearance time could be extended to several hours. We further found that after the pinholes in a given scanned area disappeared, we observed no more pinholes in that area for the same scan parameters (i.e. imaging-force, voltage). We observed these

phenomena multiple times for each sample at several bias-voltages in the range -1V to +1V. The topographic images were not observed to change over any measured timescale.

From this experiment we conclude: (1) Since the disappearance time is affected by the oxygen percentage, pinhole disappearance is attributed to oxidation. (2) Since our samples had been stored in air for weeks before study, features observed to have an oxidation time of order minutes must have been created by the scanning of the tip. *Thus, CAFM current maps should generally be viewed as pinhole susceptibility maps, where the pinholes under study are created during the scanning.* (3) Once potential pinholes in a given scan area have been created and subsequently oxidized, the pinhole susceptibility for that area is significantly reduced. (4) Given differing oxidation times between samples, and the fact that the oxidation time is of order the imaging time, it is difficult to intercompare current maps taken on samples exposed to air for periods of order the oxidation time or less. Although such maps might reveal intrinsic pinholes [17], the level of oxidation of those pinholes would vary between samples in an unknown fashion.

One question arising upon consideration of this experiment is the affect of continuously scanning the sample while measuring the oxidation time. One might suggest that the scanning creates the observed oxidation, and indeed, anodic oxidation, in which a CAFM tip actually induces local oxidation of the surface, is a well known phenomena.

However, many studies on aluminum oxide and other materials show that anodic oxidation takes place only when 1) the sample is positively biased with respect to the tip, and 2) the bias voltage exceeds a certain threshold, which for aluminum oxide is 4V [18].

In addition, anodic oxidation produces significant topographic features. Given our observation of pinhole oxidation at both negative and positive sample bias, at voltages significantly less than the anodic oxidation threshold, and with no topographic signature, we do not believe that the observed oxidation is related to tip-induced anodic oxidation as detailed in the literature.

The implications of this experiment for CAFM measurements are as follows. One intriguing intimation of this experiment for device performance is suggested by the inability to create further pinholes in a given area once it has been scanned. If devices can be improved with pinhole-impervious barriers, this experiment suggests a means to create such barriers. Although we have not yet further explored this implication, we reemphasize it here as a potentially interesting topic for further study.

The primary implication of this experiment is that for CAFM in air, current images should be interpreted as pinhole susceptibility maps. For comparison between maps, the exposure time of the sample to air should be considered. One straightforward method to achieve consistent comparisons between maps is to take data many oxidation time constants after fabrication on an area which has not been previously scanned. This is the method employed herein. A UHV study may permit measurement of intrinsic oxide properties if the sample is grown and studied in-situ and never exposed to air. In this case, CAFM measurements for many imaging conditions are presumably also pinhole susceptibility maps, although this may not be apparent in the absence of an oxidation time constant. However, by making measurements in air such as those described above,

one could establish voltage and imaging-force parameters which do not create pinholes, and using these, measure intrinsic properties in UHV.

In Fig. 2 we present data to determine the dependence of current measurements on cantilever deflection/imaging force and to assess the statistical reproducibility of current measurements. Each data point in the figure represents statistics from a distinct current map such as those shown in Fig. 1. All maps were taken on the same sample (s2), which was fabricated a month before the initial study. The maps were taken over the period of a month with different cantilevers, as indicated.

Focusing first on the data represented by circles, we find that for a single cantilever the statistical properties of a current map depend greatly on cantilever deflection/imaging force. A larger imaging force results in a broader current distribution (Fig. 2a), higher measured currents (Fig. 2b, closed) and more area with measurable current (Fig. 2b, open). These observations can be seen in the raw data by comparing the current maps of Fig 1: a/b/c with those of Fig. 1:e/f/g, respectively.

The observations reported in the previous paragraph demonstrate cleanly and definitely that imaging force profoundly affects current maps in CAFM. All the circle data of Fig. 2 was taken with the same cantilever, on the same sample, and on the same day. In addition, these maps were taken in a random order with respect to deflection to rule out any tip wear effects during imaging. Thus, the only parameter varied between successive current maps was the cantilever deflection, x , which is simply related to the imaging

force by the cantilever's spring constant, k , according to the relation $F=kx$. Given this, the data clearly show that imaging force must be controlled in order to make consistent CAFM current measurements.

The circle data of Fig. 2 further demonstrate that if the imaging force is controlled, then statistically reproducible current measurements can be made with a given cantilever. To further quantify reproducibility, consider that for individual pinholes tracked for an hour in 15 sequential images on the same area (in 5 % oxygen, which gives an oxidation time of several hours), the maximum measured current on a given pinhole ($\equiv I_m$) varied by approximately $\pm 0.5 \langle I_m \rangle$. This variation in measurement on individual features is consistent with the statistical scatter observed in Fig. 2. These observations establish a criterion for statistical reproducibility of CAFM measurements. While this criterion may appear permissive, we demonstrate in Fig. 1 that the measured difference from sample to sample significantly exceeds this statistical variation.

In Fig. 2 we also plot data taken with three other cantilevers. While the current data taken with cantilevers from the same wafer (triangles) fall reasonably within the scatter of the circle data, the data taken with a cantilever from a different wafer (squares) do not. This disparity is probably due to a significantly different spring constant, and hence imaging force, for this cantilever. This observation reemphasizes the importance of controlling the imaging *force* in order to make consistent CAFM current measurements. We found that the topographical images did not depend on either the imaging force or the particular cantilever used.

The dependence of current on imaging force has been observed in CAFM studies of many materials [1,13,19,20,21] and was investigated extensively in Ref. 14, in which it was suggested that the dependence arises from a change in the effective tip-sample contact area. Given the demonstrated substantial variation of current with imaging force, we suggest that the significant disparities between previous CAFM measurements [7,8,9,10] on comparable samples of AlO_x arise from the use of different imaging forces in the studies. To facilitate comparison of results between research groups, we suggest that in future CAFM studies at least an estimate of this critical variable be reported. In response to the studies we report herein, we are working on a means to measure cantilever spring constants *in situ*, and these results will be reported in a future paper. Given the uncertainties in cantilever spring constants, it may be nonetheless difficult to compare absolute results between groups. However, within a single research group this problem may be addressed by using the same cantilever, or cantilevers from a single wafer, to make relative comparisons between samples.

Comparison from row to row of Fig. 1 demonstrates that such relative comparisons of pinhole susceptibility from sample to sample are independent of the absolute imaging force employed. For example, sample s3 clearly shows markedly higher coverage of conducting regions than either of the other samples at both cantilever deflections [22]. Given our interpretation of conducting regions, we can then conclude that our samples fabricated by evaporation from an effusion cell in UHV have the highest susceptibility to the creation of local pinholes of any samples studied.

More generally, Fig. 1 demonstrates that samples fabricated by different methods show distinctive topographies and current/pinhole-susceptibility maps. The further ability to relatively rank the fabrication methods by their propensity to produce pinholes in the barrier, suggests the utility of using CAFM for rapid characterization of fabrication methods, if a correlation between macroscopic qubit performance and this ranking can be established. Preliminary experiments show such a correlation, and further experiments are underway to substantiate this observation generally.

In summary, conducting atomic force microscopy is a potentially powerful tool for studying the nanometer-scale electrical properties of tunnel junction oxide-barriers. Care must be taken to interpret the images in the appropriate physical context since under usual imaging conditions CAFM gives pinhole susceptibility rather than intrinsic conductance. In addition, the imaging force needs to be controlled to make consistent and valid intercomparisons of data. Given these considerations, CAFM topographies and current maps produce repeatable and dissimilar measurements for samples fabricated in different ways. Given the importance of insulating oxides in solid state devices and the growing need to characterize these materials on a short length scale, CAFM, with its nanometer spatial resolution and capacity for imaging insulators, provides a unique tool for understanding and improving these materials and devices.

Acknowledgements: We thank E.W. Hudson, Sae Woo Nam, and J. Ullom for helpful discussions. This work is supported in part by NSA/ARDA.

-
- ¹ S. J. O'Shea, R. M. Atta, M. P. Murrell, and M. E. Welland, *J. Vac. Sci. Technol. B* **13**, 1945 (1995).
- ² R. W. Simmonds, K. M. Lang, D. A. Hite, D. P. Pappas, and John M. Martinis, Preprint.
- ³ G. Ceballos, Z. Song, J. I. Pascual, H. -P. Rust, H. Conrad, M. Bäumer, and H. -J. Freund, *Chem. Phys. Lett.* **359**, 41 (2002).
- ⁴ O. Kizilkaya, D. A. Hite, D. M. Zehner, and P. T. Sprunger, *Surf. Sci.* **529**, 223 (2003).
- ⁵ W. H. Rippard, A. C. Perrella, F. J. Albert, and R. A. Buhrman, *Phys. Rev. Lett.* **88**, 046805-1 (2002).
- ⁶ K. M. Mang, Y. Khang, Y. J. Park, Young Kuk, S. M. Lee, and C. C. Williams, *J. Vac. Sci. Technol. B* **14**, 1536 (1996).
- ⁷ Y. Ando, H. Kameda, H. Kubota, and T. Miyazaki, *J. Appl. Phys.* **87**, 5206 (2000).
- ⁸ V. Da Costa, C. Tiusan, T. Dimopoulos, and K. Ounadjela, *Phys. Rev. Lett.* **85**, 876 (2000).
- ⁹ E. Z. Luo, S. K. Wong, A. B. Pakhomov, J. B. Xu, I. H. Wilson, and C. Y. Wong, *J. Appl. Phys.* **90**, 5202 (2001).
- ¹⁰ Alexander Olbrich, Bernd Ebersberger, Christian Boit, Johann Vancea, Horst Hoffmann, Hans Altmann, Guenther Gieres, and Joachim Wecker, *Appl. Phys. Lett.* **78**, 2934 (2001).
- ¹¹ Alexander Olbrich, Bernd Ebersberger, and Christian Boit, *Appl. Phys. Lett.* **73**, 3114 (1998).
- ¹² S. J. O'Shea, R. M. Atta, and M. E. Welland, *Rev. Sci. Instrum.* **66**, 2508 (1995).

¹³ M. A. Lantz, S. J. O'Shea, and M. E. Welland, *Rev. Sci. Instrum.* **69**, 1757 (1998).

¹⁴ M. A. Lantz, S. J. O'Shea, and M. E. Welland, *Phys. Rev. B* **56**, 15345 (1997).

¹⁵ K. M. Lang, S. Nam, J. Aumentado, C. Urbina, and John M. Martinis, *IEEE Trans. Appl. Supercond.* **13**, 989 (2003).

¹⁶ Certain commercial instruments are identified to specify the experimental study adequately. This does not imply endorsement by NIST or that the instruments are the best available for the purpose.

¹⁷ We define an intrinsic pinhole as one which is present in the as-grown sample and not created by the scanning of the tip.

¹⁸ E. S. Snow, P. M. Campbell, and D. Park, *Superlattices and Microstructures* **20**, 545 (1996).

¹⁹ J. T. Dickinson, L. C. Jensen, K. H. Siek, and K. W. Hipps, *Rev. Sci. Instrum.* **66**, 3802 (1995).

²⁰ P. De Wolf, J. Snauwaert, T. Clarysse, W. Vandervorst, and L. Hellemans, *Appl. Phys. Lett.* **66**, 1530 (1995).

²¹ J. G. Park, S. H. Lee, B. Kim, and Y. W. Park, *Appl. Phys. Lett.* **81**, 4625 (2002).

²² The observant reader might notice a correlation between increased topographic roughness and greater pinhole susceptibility for the particular maps of Fig. 1. Having looked at several samples fabricated by other means, we do not observe this correlation to be universal.

²³ With the exception of s1, the statistical properties of a pinhole susceptibility map stayed substantially the same with the time the sample spent stored in air. For s1, it was possible to create a relatively small number of pinholes within ~ 1 day of sample

fabrication and exposure to air, after which it was no longer possible to create any pinholes for $V < 5V$ and cantilever deflection $< 25nm$. For consistency, all maps in Fig. 1 were taken several weeks after sample fabrication, and hence s1 shows no pinholes in these maps.

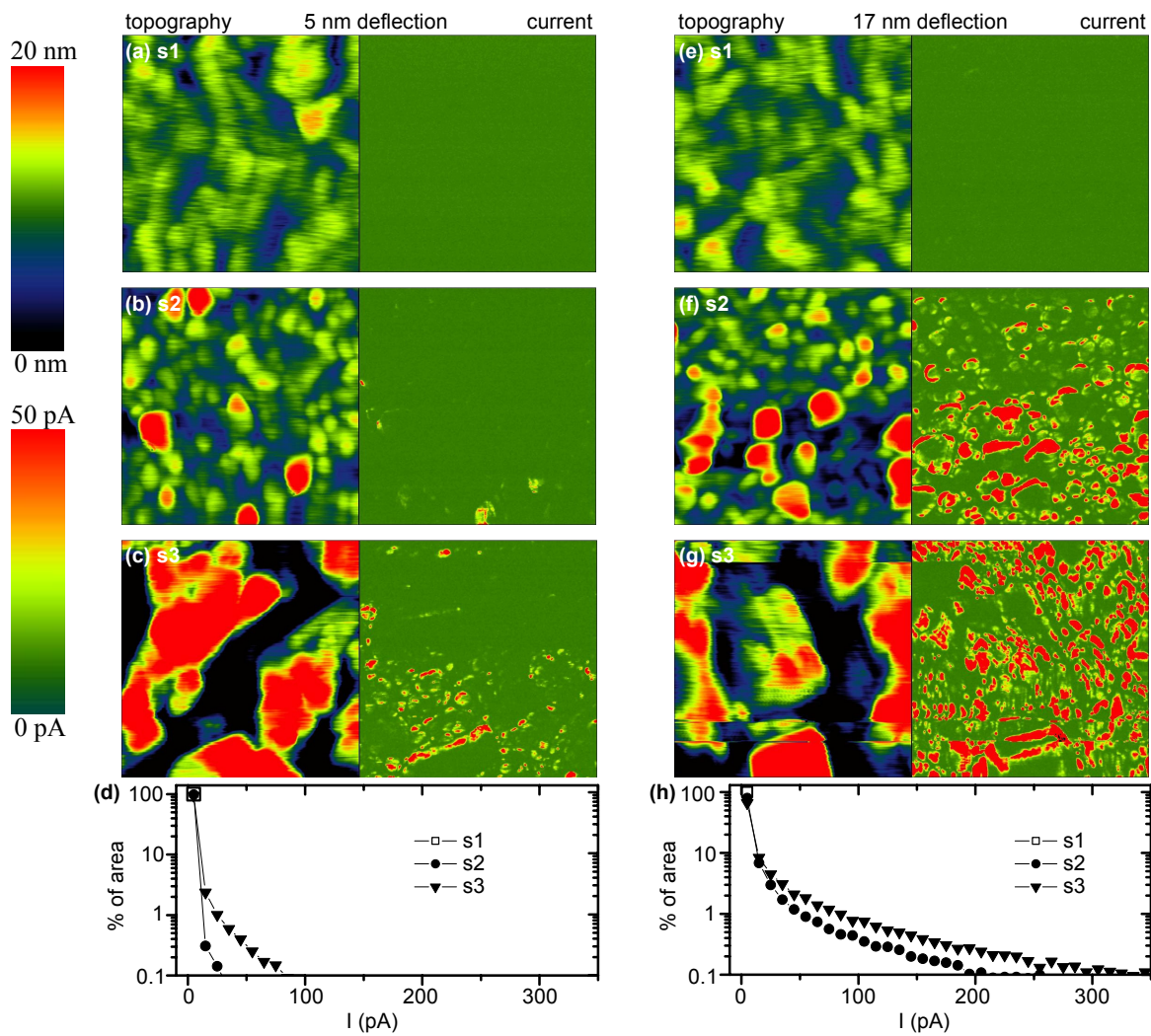
Sample	Substrate	Al Deposition Conditions			RMS Roughness (nm)
		Al Source	Gas in Chamber	Pressure (mT)	
s1	Si +SiO ₂	sputter	Ar	5	1.8
s2	Si +SiO ₂	sputter	Ar/O ₂	5/0.1	4.4
s3	Si(100) - (2x1)	evaporate from effusion cell	UHV	10 ⁻⁷	11.4

K.M. Lang
Table I
1 column

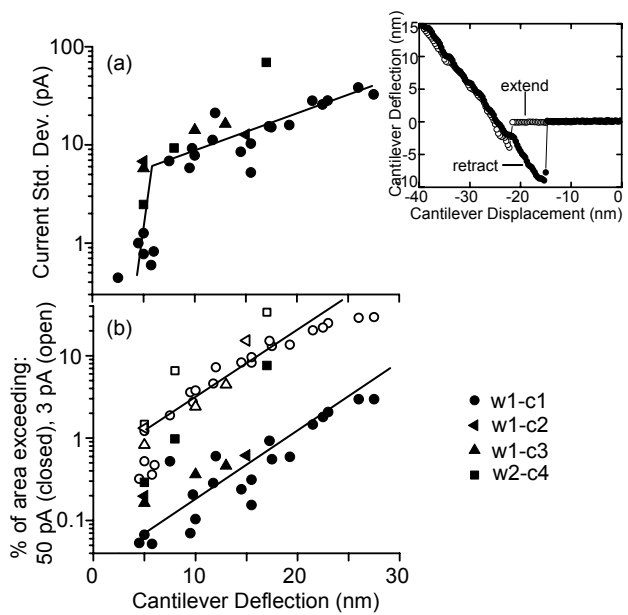
TABLE I: Fabrication details and surface roughness for samples studied. The roughness is defined as the average standard deviation of topographies taken on the sample.

FIG. 1 (color): Topography (left) and simultaneous current maps (right) of several AlO_x samples taken at two different deflection setpoints. All maps were taken on a 500 x 500 nm² area with 256² pixels at sample bias -1 V. The images in the left and right column were taken with cantilever deflection setpoints of 5 nm and 17 nm respectively. The bottom panels show the histogram of current values present in the maps of the respective columns. [23]

FIG. 2: Dependence on cantilever deflection of the statistical properties of current maps demonstrating the significant influence of imaging force. Each data point represents statistics for an entire current map taken on a 500 x 500 nm² area of sample s2 with 256² pixels at sample bias -1 V. The cantilever deflection for each map is measured as in the inset. The maps were taken with four different cantilevers (c#) fabricated on two wafers (w#) as indicated in the legend. In (a) a small number of points (~50) at very large currents (>1nA) are excluded from the calculation since they mostly represent displacement currents arising when the tip is tracking poorly. The lines are guides to the eye.



K.M. Lang
 Figure 1
 2 column



K.M. Lang
 Figure 2
 1 column